Physical Properties of the *Escherichia coli* Transcription Termination Factor Rho. 1. Association States and Geometry of the Rho Hexamer†

Johannes Geiselmann,‡ Thomas D. Yager,§ Stanley C. Gill,‖ Patrick Calmettes,⊥ and Peter H. von Hippel*
Institute of Molecular Biology and Department of Chemistry, University of Oregon, Eugene, Oregon 97403
Received May 13, 1991; Revised Manuscript Received August 22, 1991

ABSTRACT: To function as a DNA–RNA helicase in rho-dependent transcript termination, six genetically identical subunits of the *Escherichia coli* transcription termination protein rho must first assemble into a hexameric complex. To help determine the quaternary structure of this complex, we have studied the association equilibria of the rho protomers. Sedimentation equilibrium, sedimentation velocity, diffusion, X-ray scattering, and neutron-scattering data have been combined to create a "phase diagram" of the association states of this protein as a function of protein concentration and ionic environment. The results show that rho exists predominantly as a hexamer under approximately physiological conditions and that this hexamer is in equilibrium with both lower and higher states of association that may also have physiologicial relevance. Small-angle X-ray scattering measurements and theoretical calculations indicate that the rho hexamer has a radius of gyration of 50 ± 3 Å. The radius of gyration measured by small-angle neutron scattering in ^2H_2O is 47 ± 3 Å. These scattering studies also support earlier models of rho as a planar hexagon which have been developed on the basis of electron microscopy. In the following paper in this issue [Geiselmann, J., Seifried, S. E., Yager, T. D., Liang, C., & von Hippel, P. H. (1992)], these results are combined with information on symmetry, subunit interactions, and packing geometry to obtain a model of the quaternary structure of the functional rho hexamer.

The *Escherichia coli* transcription termination factor rho is required for specific termination of many RNA transcripts [for reviews, see Platt and Bear (1983), von Hippel et al. (1984), Platt (1986), Yager and von Hippel (1987), and Bear and Peabody (1988)].

Rho-dependent termination appears to involve two mechanistically distinct steps, each of which confers partial specificity on the process. (i) The transcriptional elongation complex pauses in its movement along the DNA template at positions that have the potential to become specific rho-dependent termination sites. The duration of these pauses may be 100-fold longer than the average "dwell time" of the transcription complex at a DNA template position during RNA transcript elongation. The factors that specify these pause sites and their durations have not yet been fully defined. Presumably interactions between the core polymerase, the DNA template, and the nascent RNA are involved, since this pausing does *not* depend on the presence of the rho protein (Reisbig & Hearst, 1981; Morgan et al., 1983a,b, 1984).

(ii) The other determinant of specificity in rho-dependent transcription termination is the binding of rho protein to specific sites on the nascent RNA transcript. This reaction also is not fully understood. The main requirement appears to be for a binding sequence on the nascent transcript that is 70 or more nucleotide residues in length and free of stable secondary structure (Morgan et al., 1985). Specific sequence preferences may be superimposed on this basic requirement (Sharp & Platt, 1984; Chen et al., 1986). Rho interacts as a hexameric complex with its binding site on the RNA (Finger & Richardson, 1982). This binding event activates an RNA-dependent ATPase activity and ultimately leads to the release of the nascent RNA from the transcription complex.

A major goal of research on rho-dependent transcription termination is to elucidate the molecular mechanism of the specific RNA-release process. Rho consists of a single type of protein subunit (protomer) encoded by a single gene in *E. coli*. However, its RNA-release function depends critically on the assembly of rho protomers into a hexameric structure (Finger & Richardson, 1982). Thus, to understand its termination function, rho must be thoroughly characterized at the level of quaternary structure in the functional state. As an initial step in this direction, we have studied the self-association behavior of the protein under different solution conditions.

We have examined the self-association behavior of rho as a function of protein and salt concentrations, and in the absence and presence of RNA cofactors (or their DNA analogues). We show that homogeneous hexamers and dodecamers of rho can form under certain well-defined conditions. The hexamer is thought to be the association state that catalyzes ATP hydrolysis (Finger & Richardson, 1982) and may also be the predominant state in vivo. Other association states also coexist in solution, and their study provides insight into the various protomer–protomer interactions that stabilize the functional rho hexamer. We have also determined the molecular weights and approximate three-dimensional shapes of the rho hexamer and dodecamer by a combination of diffusion, sedimentation velocity and equilibrium, and X-ray and neu-

† This work has been submitted (by J.G.) to the Graduate School of the University of Oregon in partial fulfillment of the requirements for the Ph.D. degree of Chemistry. These studies were supported in part by USPHS Research Grants GM-15792 and GM-29158 (to P.H.v.H.), by NIH Individual Postdoctoral Fellowship GM-10227 (to T.D.Y.), and by a grant from the Lucille P. Markey Charitable Trust. P.H.v.H. is an American Cancer Society Research Professor of Chemistry.

* To whom correspondence should be addressed.
‡ Present address: Unité de Physicochimie des Macromolécules Biologiques, Institut Pasteur, 25 rue du Dr. Roux, 75724 Paris, Cedex 15, France.
§ Present address: NSF Center for Molecular Biotechnology, Division of Biology (139-74), California Institute of Technology, Pasadena, CA 91125.
‖ Present address: Department of Chemistry and Biochemistry, University of Colorado, Boulder, CO 80309.
⊥ Address: Laboratoire Léon Brillouin, CEN-Saclay, 91191 Gif-sur-Yvette Cedex, France.

0006-2960/92/0431-111$03.00/0

tron-scattering measurements. These measurements, when combined with electron microscopy (Bear et al., 1988; Gogol et al., 1991), also provide information about the relative positions of the rho protomers in the hexamer, as well as in other stable association states. In the following paper in this issue (Geiselmann et al., 1992), we establish the symmetry and packing geometry of the rho hexamer, thus completing a low-resolution assignment of its quaternary structure.

Materials and Methods

Reagents and Buffers. All solutions were prepared with redistilled water or water that had been purified with a Barnstead Nanopure II system. All buffers, salts, and organic chemicals were purchased from Sigma unless otherwise indicated. Rho protein was prepared in TEGD buffer, which contains 10 mM Tris-HCl (pH 7.7), 0.1 mM EDTA, 0.1 mM DTT, 5% (v/v) glycerol, and KCl at the concentrations listed below. "Storage buffer" contains 20 mM Tris-HCl (pH 7.9), 0.1 mM EDTA, 0.1 mM DTT, 100 mM KCl, and 50% (v/v) spectral grade glycerol. The buffer used in most of the experiments described in this paper contains 40 mM Tris-HCl (pH 7.8), 0.1 mM EDTA, 10 mM $MgCl_2$, and 100 mM KCl, plus supplements as listed below. The absence or presence of DTT in the buffers does not appear to be critical. This is not unexpected, since the rho monomer contains only a single (nonessential) cysteine residue (Seifried et al., 1988; Dombrowski & Platt, 1988).

Preparation of $(dC)_{20}$. The single-stranded DNA oligonucleotide $(dC)_{20}$ was synthesized in the University of Oregon Biotechnology Laboratory using an Applied Biosystems automated DNA synthesizer and phosphoramidite chemistry. After removal of the trityl group, the $(dC)_{20}$ was purified by reverse-phase HPLC, lyophilized, and stored as a dry powder at −10 °C. A molar extinction coefficient ($\epsilon_{M,266}$) of 1.52×10^5 M^{-1} cm^{-1} (Adler et al., 1967) was used for $(dC)_{20}$.

Purification of Rho. E. coli strain AR120 was transformed with plasmid p39-AS and grown as described by Mott et al. (1985). Overproduction of rho was induced by the addition of nalidixic acid. The protein was purified according to Mott et al. (1985), with the following modifications. Rho-containing fractions from the Bio-Rex 70 column were pooled. The pool was diluted with TEGD buffer (minus KCl) until its conductivity decreased to 7.2×10^{-3} mho. This solution was then loaded onto a heparin-agarose column in TEGD, and the rho protein was eluted with a gradient of 0.2–0.8 M KCl in TEGD. The rho peak was dialyzed into TEGD containing 0.1 M KCl and loaded onto a PUP [agarose 5-[(4-aminophenyl)-phosphoryl]uridine 2′(3′)-phosphate] column. Elution was performed with a gradient of 0.1–0.5 M KCl in TEGD. If maximum purity rho was desired, the eluent was then concentrated by ammonium sulfate precipitation and refractionated on a 2.5 cm × 120 cm Bio-Gel A5M gel filtration column in TEGD containing 0.1 M KCl. The final purified rho was dialyzed into storage buffer. When analyzed on an 8% SDS–polyacrylamide gel, the rho protein appeared >98% pure by Coomassie blue staining. Silver staining revealed a few contaminant bands in trace amounts.

Extinction Coefficient of Rho and Spectral Measurements. The concentration of rho must be known with high accuracy and precision if one is to conduct meaningful binding or titration studies. We have carefully determined the extinction coefficient of rho using a modification of the Edelhoch (1967) method (Gill & von Hippel, 1989). Using a 1% (w/v) solution, we have experimentally determined the extinction coefficient of rho (in mass concentration units) to be $E_{m,280} = 0.325$ $(mg/mL)^{-1}$ cm^{-1}. Taking the molecular weight of the rho protomer as 46 974 from the DNA sequence (Pinkham & Platt, 1983), we calculate the molar extinction coefficient to be $\epsilon_{M,280} = 1.53 \times 10^4$ M^{-1} cm^{-1}.

Table I: Properties of the Rho Hexamer

molecular weight	
sedimentation–diffusion	287 000 ± 20 000
equilibrium ultracentrifugation	286 000 ± 10 000
forward X-ray scattering	285 000 ± 15 000
forward neutron scattering in ^2H_2O	285 000 ± 25 000
calculated (from DNA sequence)	282 000
extinction coefficient	
mass ($E_{m,280}$)	0.325 $(mg/mL)^{-1}$ cm^{-1}
molar ($\epsilon_{M,280}$)	1.5×10^4 M^{-1} cm^{-1}
partial specific volume	
measured in 0.1 M KCl	0.755 ± 0.003 cm^3/g
measured in 0.5 M KCl	0.751 ± 0.002 cm^3/g
measured in 50 mM KH_2PO_4	0.745 ± 0.002 cm^3/g
calculated	0.745 cm^3/g
sedimentation coefficient ($S_{20,w}$)	10.4 ± 0.2 S
diffusion coefficient ($D_{20,w}$)	$3.4 \pm 0.1 \times 10^{-7}$ cm^2/s
radius of gyration (R_G)	
X-ray scattering	50 ±3 Å
neutron scattering	47 ±3 Å
calculated from model (Figure 7)	49 Å
approximate shape (from EM, SAXS, SANS)	regular (planar) hexagon (some departure from planarity is allowed)

The extinction coefficient of rho had previously been estimated as $E_{m,280} = 0.37$ $(mg/mL)^{-1}$ cm^{-1} from amino acid analysis data (Finger & Richardson, 1981). This early estimate is 14% higher than our present value. The new value is based on *exact* knowledge of the amino acid composition obtained from the DNA sequence of the gene. Using the new value, we obtain excellent agreement between the theoretical and the measured molecular weights of the rho hexamer (see Table I). Thus our new determination of the extinction coefficient appears to be more accurate than the earlier estimate of Finger and Richardson (1981). We note that the use of this new value of the extinction coefficient requires minor corrections in all concentration-dependent physical parameters for rho that have been reported in the literature.

Absorbance spectra of rho were measured with a Hewlett Packard 8450 spectrophotometer. Spectra (220–400 nm) were corrected for light scattering using an inverse-fourth-power law for the dependence of the scattered light intensity on wavelength. At 280 nm, the light scattering correction was about 6% of the measured absorbance.

Partial Specific Volume. The partial specific volume of rho must be known for accurate molecular weight calculations to be made from sedimentation and scattering data. We have determined the partial specific volume of rho using an Anton-Parr vibrating cell densimeter. The densimeter was calibrated with distilled water and dry air at known atmospheric pressure. The temperature within the densimeter cell was controlled to ±0.01 °C by use of an external water bath and by placing the apparatus and the water bath in a constant temperature room.

To test the accuracy of the densimeter and of our technique, the densities of 0.500 M KCl (Radiometer Copenhagen lot no. 955-020) and 0.300 M NaCl (J. T. Baker lot no. 414128) were determined. Salt solutions were prepared gravimetrically from salt crystals dried in a vacuum oven for 2 h at 150 °C. The measured densities of these salt solutions showed deviations of less than 0.2% from the values in standard reference tables (Weast, 1978). As an additional test, we made six determinations of the partial specific volume of bovine serum albumin (BSA), Sigma product A-0281, lot no. 35F-942, used without further purification. In our determinations the BSA

was at a concentration between 2.2 and 4.4 mg/mL. An extinction coefficient $E_{m,280} = 0.658$ (mg/mL)$^{-1}$ cm^{-1} was assumed for BSA (Nolken & Timasheff, 1967), and all measurements of UV spectra were corrected for light scattering as described above. We obtained $\bar{\nu}_2 = 0.720 \pm 0.002$ cm^3/g, as compared with the published value of $\bar{\nu}_2 = 0.734$–0.735 cm^3/g (Reisler & Eisenberg, 1969; Lee & Timasheff, 1974).

To determine the partial specific volume of rho, the protein was dialyzed extensively into one of the following buffers: (i) 0.1 M KCl, 10 mM Tris, and 1 mM EDTA (pH 7.7); (ii) 0.5 M KCl, 10 mM Tris, and 1 mM EDTA (pH 7.7); (iii) 50 mM $KHPO_4$ (pH 7.7). Rho concentrations were determined spectrophotometrically as described above. We assume that $\bar{\nu}_2$ does not depend on the concentration of rho. Our experimental results are summarized in Table I. We have used $\bar{\nu}_2 = 0.75$ cm^3/g in all computations of the molecular weight of rho. We note that a 1% error in $\bar{\nu}_2$ translates into approximately a 3% error in molecular weight as measured by equilibrium sedimentation or sedimentation/diffusion techniques.

Equilibrium Ultracentrifugation. Sedimentation equilibrium experiments were performed using a Beckman model E analytical ultracentrifuge as described by Chervenka (1965) and Van Holde (1967). The high speed (meniscus depletion) method was used in all runs. About 0.12 mL of a 0.5 mg/mL solution of rho (without a supporting layer of oil) was loaded into one sector of a 12-mm path length double-sector cell equipped with sapphire windows, and a slightly larger volume of buffer was loaded into the other sector. The speed of centrifugation was set high enough to fully deplete the cell's meniscus region of protein. Interference fringe patterns were photographed on Kodak Metallographic plates after equilibrium had been reached (about 2 days after the start of a run). The photographic plates were analyzed with a Nikon Shadowgraph comparator, following the procedure of Van Holde (1967). The homogeneity and weight-average molecular weight M_w of each sample were estimated using (Chervenka, 1965; Van Holde, 1967)

$$M_w = [2RT/\omega^2(1 - \bar{\nu}_2\rho)][\mathrm{d} \ln \Delta j/\mathrm{d}r^2] \quad (1)$$

where ω is the angular velocity, $\bar{\nu}_2$ is the partial specific volume of the protein, ρ is the solution density, R is the universal gas constant, and T is the absolute temperature. In the meniscus depletion method, the fringe displacement Δj is directly proportional to the weight concentration of the protein c at a given radial distance r.

Velocity Sedimentation. We also used a Beckman model E analytical ultracentrifuge to examine the velocity sedimentation behavior of rho in various buffers. Rotor speeds ranging from 32000 to 40000 rpm were used, and scans were taken every 12 min. The shapes of the UV-absorbing sedimentation boundaries were recorded on thermal paper with the photoelectric scanner, usually at a wavelength of 280 nm. The paper traces were digitized with a Hewlett-Packard digitizing board. Approximately 300 points were taken across each boundary, and the resultant data were stored for subsequent analysis.

The shape of each sedimentation boundary was analyzed by the method of Van Holde and Weischet (1978). This method corrects for diffusional spreading and yields a distribution of sedimentation coefficients across the boundary. The method can often discriminate between homogeneous and polydisperse samples, provided that the different molecular species in a polydisperse sample do not equilibrate faster than the time scale of the sedimentation run, i.e., within minutes. In our application of the method, we divided the sedimentation boundary into 15 equally spaced intervals. The apparent sedimentation coefficient S_{app} was calculated at each point between adjacent intervals and was plotted as a function of $t^{-1/2}$, where the elapsed time t is defined relative to an extrapolated zero time for the run [see Van Holde and Weischet (1978)]. Each set of points describing S_{app} as a function of $t^{-1/2}$ was extrapolated to infinite time by a linear least-squares procedure to correct for diffusional effects. If the lines of extrapolation converge as $t^{-1/2}$ approaches zero, then we can conclude either that the solution contains material of homogeneous molecular weight or that it contains a mixture of rapidly equilibrating components of different molecular weights. All reported sedimentation coefficients were corrected to standard conditions (water at 20 °C).

Definition of Scattering Vector. In this work, we have employed the techniques of quasielastic light scattering, X-ray scattering, and neutron scattering. To avoid confusion, we will consistently use the following formula for the scattering vector q:

$$q = (4\pi n/\lambda) \sin \theta \quad (2)$$

where n is the refractive index (approximately 1 for neutrons and X-rays). The scattering angle 2θ is defined as the angle between the incident and the scattered beams.

Quasielectric light scattering, X-ray scattering, and neutron scattering utilize different wavelengths of radiation and consequently different ranges of the scattering vector. For our QLS studies, a wavelength of 514.5 nm was used, and the scattering angle was varied from 30° to 145°. A wavelength of 0.154 nm was used in the X-ray scattering experiments, and the scattering vector was varied approximately from 0.05 to 0.95 nm^{-1}. Finally, in the neutron-scattering studies, two different sets of wavelengths and scattering vectors were employed. In one set of experiments, the wavelength was 0.5 nm and the scattering vector varied from 0.21 to 2.21 nm^{-1}. In the second set of experiments, the wavelength was 1.3 nm, and the scattering vector varied from 0.045 to 0.48 nm^{-1}.

Quasielastic Laser Light Scattering. The translational diffusion coefficient of rho was estimated from autocorrelation analysis of the quasielastically scattered light. The 514.5-nm line of an argon ion laser (Spectra Physics model 5) was used in the TEM_{00} mode. An intracavity etalon was used to select a single longitudinal mode of laser light. The output power of the laser beam was adjusted to lie between 5 and 500 mW, depending on the concentration of rho that was used in each experiment. Each sample of rho was passed through a 0.22-mm filter (Millipore Millex-GV) directly into an optical cell that had been washed extensively with filtered water. No detectable loss of protein occurred during filtration. The optical cell was mounted in a water-cooled goniometer head that was connected to a thermostated circulating water bath. The temperature at the outer edge of the cell was measured to ±0.1 °C with a calibrated Hg thermometer and was held constant to ±0.05 °C during the data collection period. The homodyne mode of light detection was used [see Berne and Pecora (1976) and Bloomfield and Lim (1978) for reviews]. Autocorrelation analysis of the scattered light was conducted in real time using an 80 channel autocorrelator (Langley-Ford model no. 1096).

The "cumulant expansion" method was used to analyze the autocorrelation function of the scattered light (Koppel, 1972; Chu, 1974; Bloomfield & Lim, 1978). The first-order autocorrelation function $g(A)$ is expanded as a power series in A:

$$g(A) = (1 + \mu A^2/2 + \ldots)e^{-\gamma A} \quad (3A)$$

where A is the lag time, μ is the quadratic coefficient of the

expansion, and γ is the mean autocorrelation decay constant. The constant γ is related to the Z-average translational diffusion coefficient D_Z as follows:

$$D_Z = \gamma/q^2 \tag{3B}$$

where q is defined by eq 2.

The polydispersity index is defined as μ/γ^2. If this index is greater than 0.1, the solution is considered to be polydisperse. Rapid equilibration between species with significantly different D_Z values can be revealed by a large polydispersity index (Bloomfield & Lim, 1978).

Interpretation of Sedimentation Velocity and QLS Data. The hydrodynamic behavior of a homogeneous macromolecule can be partially described with

$$S_{20,w} = M_w(1 - \bar{\nu}_2\rho)/Nf \tag{4A}$$

and

$$D_{20,w} = RT/Nf \tag{4B}$$

Here N is Avogadro's number, and f is the translational frictional coefficient. The symbol $D_{20,w}$ represents the Z-average diffusion coefficient, D_Z, after correction to standard conditions (water at 20 °C). For a monodisperse system, eqs 4A and 4B can be combined in the Svedberg equation to yield the molecular weight (M) of a homogeneous species:

$$S_{20,w}/D_{20,w} = M(1 - \bar{\nu}_2\rho)/RT \tag{4C}$$

The Svedberg equation should not be used to calculate an apparent molecular weight of a polydisperse sample. This follows because the sedimentation and diffusion coefficients, as measured by the above techniques, represent differently weighted averages in eq 4C. The sedimentation coefficient is a weight-average parameter (Schachman, 1959), while the diffusion coefficient, as we have stated, is a Z-average parameter (Bloomfield & Lim, 1978).

The translational frictional coefficient (f) of a multimeric species can be related to that of a spherical protomer (f_o) with (Bloomfield et al., 1967)

$$f = mf_o[1 + (a/m)\sum_{i\neq j}^{m}\sum^{m}(1/r_{ij})]^{-1} \tag{4D}$$

Here m is the number of monomers in the multimer, a is the radius of the monomer, and r_{ij} is the distance between the centers of monomers i and j.

Small-Angle X-ray Scattering (SAXS). The LURE synchrotron (Orsay, France) was used as a source of pulsed X-rays with λ = 0.154 nm. With the storage ring running at 1.72 GeV and 180–220 mA, the flux of the singly focused monochromatic beam was approximately 10^9 photons/s. The beam gave a spot approximately 1 mm in diameter at the sample plane. This spot is practically equivalent to a point source. A 2-mm detector slit was used. The camera has been described by Depautex et al. (1987). Scattering was monitored with a position-sensitive delay-line detector (Gabriel et al., 1978). The scattering vector (q) is defined by eq 2. The raw data, $I(q)$, were stored directly in the 4000 channel memory of a Tracor Northern TN 1710 multichannel analyzer. The data acquisition system has been described by Boulin et al. (1986).

To prepare a set of raw data for analysis, we normalize each value of $I(q)$ to the incident beam intensity. Then, to correct for background scattering, we subtract the normalized value of a buffer blank that has been measured at that q value. Data that have been processed in this way are designated $I'(q)$. No collimation correction is required since a point source and a narrow detector slit were used.

Small-Angle Neutron Scattering (SANS). The PACE neutron spectrometer (Laboratoire Leon Brillouin, Saclay, France) was used as a source of neutrons with λ = 0.5 or 1.3 nm. The instrument has been well calibrated, and absolute scattering intensities were determined by reference to the incoherent scattering of water (Calmettes et al., 1987, 1989; Kunz et al., 1990).

Samples of rho were dialyzed exhaustively into 0.1 M KH_2PO_4 and 1 mM EDTA (pH 7.7) in ^1H_2O or into 0.1 M KH_2PO_4 and 1 mM EDTA ("pH" 7.5) in ^2H_2O (as measured with a regular pH electrode that had been calibrated at pH 7.40 in buffered ^1H_2O). Samples of $(dC)_{20}$ were prepared by resuspension of dried powder in these buffers. The effective pD is 0.4 units higher than what is registered with a regular pH electrode. Thus we estimate pD to be 7.9 for the stock solutions in ^2H_2O.

Solutions of rho, or of rho + $(dC)_{20}$, of various ^2H_2O contents were prepared by gravimetric mixing of stock solutions in ^1H_2O and ^2H_2O. Matched buffers (without rho) were prepared in the same way. SANS spectra of rho, rho + $(dC)_{20}$, and buffer alone were collected. Some contamination of the ^2H_2O stock solutions with protons inevitably occurred since protonated potassium phosphate and EDTA were used in the preparation of the stock solutions. Accordingly, spectra in ^2H_2O were corrected for incoherent background scattering due to contaminant ^1H_2O and to unexchanged ^1H atoms of the solute by assuming that $I(q) \simeq 0$ for $q \simeq 2.2$ nm^{-1}. The corrected SANS spectra that result are designated $I'(q)$ (Figure 4). They have a somewhat "flattened" appearance as compared to the SAXS spectra; this, however, does not detract from the principal conclusions of our study.

Radii of Gyration. Radii of gyration (R_G) were computed from the innermost points of the ln $I'(q)$ versus q^2 curves using (Guinier & Fournet, 1955)

$$\ln I'(q) = \ln I'(0) - (1/3)(R_G q)^2 \tag{5A}$$

To calculate the radius of gyration of an assemblage of m protomers, we used the parallel axis theorem (Stockel et al., 1979; Lane, 1982):

$$R_G^2 = (3/5)a^2 + (1/m)\sum_{i}^{m} d_i^2 \tag{5B}$$

where a has been defined above and d_i is the distance between the center of a protomer i and the center of gravity of the assemblage.

Molecular Weights from Forward Scattering Intensities. In our X-ray scattering experiments, the molecular weight of rho is not determined absolutely, but only in relation to a homogeneous protein standard. We have compared the intensity of the forward scatter from solutions of rho to that of a solution of aspartyl transcarbamylase (ATCase) of known concentration (M = 300 000) to estimate the molecular weight of rho. The error in the molecular weight determined by this method is due principally to error in the spectrophotometric determination of protein concentration.

In neutron-scattering experiments, the molecular weight of rho was determined absolutely by the following approach. For sufficiently dilute solutions, the forward scattered coherent intensity $I'(0)$ is given by

$$I'(0) = (I_o VCM/N)[(\rho^N - \rho_o^N)\bar{\nu}_2]^2 \tag{6}$$

where I_o is the incident intensity, V is the scattering volume (cm^3), C is the mass concentration of solute (g/cm^3), and ρ^N and ρ_o^N are the scattering length densities (cm^{-2}) of the solute and solvent, respectively. Equation 6 allows the molecular

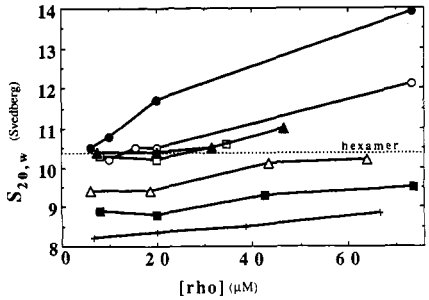

FIGURE 1: Average sedimentation coefficient of rho as a function of protein concentration and ionic environment. The sedimentation coefficient (corrected to water at 20 °C) is plotted as a function of the concentration of rho monomers. The sedimentation coefficient of the rho hexamer is indicated by the dotted line. Symbols: (●) 50 mM KCl, (○) 100 mM KCl, (▲) 50 mM KH_2PO_4 (pH 7.7), (□) 200 mM KCl, (△) 0.5 M KCl, (■) 1.0 M KCl, and (+) 1.5 M KCl.

weight of a macromolecule to be determined in an absolute sense, provided that I_0 has been measured.

Analysis of Scattering Curves beyond the Guinier Region. We have also analyzed X-ray and neutron-scattering curves at values of the scattering vector beyond the Guinier region. An experimental $I'(q)$ curve was compared to a theoretical curve that had been calculated using the Debye formula for an assemblage of m spherical protomers:

$$I(q) = [F_o(q)/m^2]\sum_i^m\sum_j^m[\sin qr_{ij}]/qr_{ij} \qquad (7A)$$

$F_o(q)$ is the form factor of an individual protomer, and r_{ij} is the distance between the centers of protomers i and j. Each protomer is considered to be a solid sphere of radius a with the following form factor:

$$F_o(q) = 3[(\sin qa) - (qa \cos qa)]/(qa)^3 \qquad (7B)$$

In this formula, the form factor has been normalized to a forward scattering intensity of unity.

RESULTS

The Association State of Rho Is a Function of Protein Concentration and Salt Concentration

If a protein can exist in several association states, the interpretation of functional assays becomes problematic. Information is required about how the association state is affected by buffer conditions, ligands, etc. We have therefore characterized the association behavior of rho as a function of protein concentration and ionic environment. In our studies the concentration of rho was varied between 0.25 and 3.4 mg/mL, which corresponds roughly to the estimated range of rho concentration in the *E. coli* cell (see Discussion). The KCl concentration was varied from 50 mM to 1.5 M, and the effects of inorganic phosphate and Mg^{2+} concentrations were also examined. Sedimentation and diffusion coefficients were used as indicators of the average degree of association (see eqs 3–4). After conditions had been found that produced a homogeneous association state, this state was examined further using the more informative techniques of sedimentation equilibrium, SAXS, and SANS.

A summary of the observed sedimentation behavior of rho is given in Figure 1. The corrected sedimentation coefficient ($S_{20,w}$) is plotted against rho concentration for a number of different buffer conditions. The horizontal dotted line divides Figure 1 into two regions, in which the sedimentation coefficient is either less than or greater than 10.4 S. (The homogeneous rho hexamer has a sedimentation coefficient of 10.4 S, as will be discussed below.)

Lower Association States of Rho. Rho protein sediments more slowly than 10.4 S when the KCl concentration is equal to or greater than 500 mM. A sedimentation coefficient of less than 10.4 S is also observed in the presence of high concentrations of Mg^{2+} (data not shown). This behavior is represented in Figure 1 by the region below the horizontal dotted line. In this region of the figure, the average association state of rho is less than hexameric. The sedimentation coefficient of a rho monomer is estimated to be about 3.4 S, assuming a roughly spherical shape and an average degree of hydration (see below). Therefore, we conclude that in this region of Figure 1 rho is *not* dissociated completely to the monomeric state.

Given that rho has an intermediate state of association (between monomeric and hexameric) in the lower region of Figure 1, we next ask whether the solution is homogeneous in this region of the phase diagram. We find that, under the conditions we have studied, rho does not exist in a monodisperse association state. In QLS experiments this inhomogeneity was revealed by a high "polydispersity index" ($\mu/\gamma^2 > 0.15$) and a strong dependence of the calculated diffusion coefficient on the scattering vector (data not shown). In sedimentation equilibrium experiments, inhomogeneity was revealed by a significant upward curvature in plots of ln Δj versus r^2 (see eq 1).

From the slopes of such plots, we infer that the *average* degree of association in this region of the phase diagram ranges between trimers and pentamers (data not shown). The identities and structures of these association intermediates of rho cannot be determined unambiguously from our sedimentation velocity, QLS, or sedimentation equilibrium data. However, in the following paper in this issue (Geiselmann et al., 1992), we demonstrate the existance of a stable dimeric association state of rho at low protein concentrations and in the presence of certain solvent perturbants. Thus, it is logical to argue that the intermediate association states we see in the experiments of this paper correspond to equilibrium mixtures of dimers, tetramers, and hexamers. Elsewhere (Gogol et al., 1991; Seifried et al., 1991) we have analyzed the association equilibria in this region of the phase diagram by cryoelectron microscopic, sedimentation, and gel filtration HPLC techniques to learn more about the intermediates in the assembly pathway of the rho hexamer.

Sedimentation velocity experiments can yield information on the rate of equilibration between different association states. The Van Holde–Weischet sedimentation analysis shows converging lines in a plot of $S_{20,w}$ vs $t^{-1/2}$ for many samples of rho that had been shown to be inhomogeneous by sedimentation equilibrium. This indicates that the various association states of rho in these samples equilibrate more rapidly than the characteristic separation times of the sedimentation velocity method (minutes).

Higher Association States of Rho. We have also examined the tendency of rho to associate beyond the 10.4 S state. Two very different types of behavior are found, depending on whether an oligonucleotide ligand (RNA or DNA) is absent or present.

In the absence of an oligonucleotide ligand, the sedimentation coefficient of rho can be increased above 10.4 S by simultaneously raising the protein concentration and lowering the concentration of KCl. This is indicated by the region in Figure 1 that lies above the horizontal dotted line. Several observations suggest that an unlimited aggregation occurs under these conditions. For example, in 50–100 mM KCl, the sedimentation coefficient of rho appears to increase without

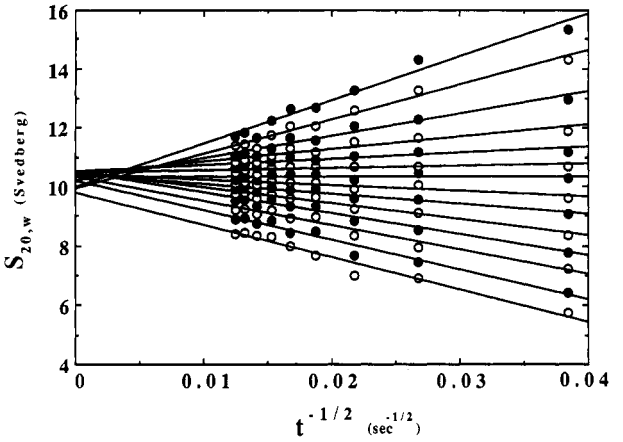

FIGURE 2: Analysis of sedimentation boundary of a 0.3 mg/mL solution of rho in 50 mM KH_2PO_4 (pH 7.7). The apparent sedimentation coefficients at 14 equally spaced points across the boundary are plotted as a function of $t^{-1/2}$. The lines at the extremes of this "fan plot" have the greatest error. An extrapolation to infinite time (y-axis intercept) yields a distribution of diffusion-corrected sedimentation coefficients across the sedimenting boundary. Convergence of the lines suggests homogeneity of the sample.

bound, with material that sediments as rapidly as 30 S being observed in a 3.5 mg/mL solution of rho in 50 mM KCl. Furthermore, on dialysis of rho from "storage buffer" into buffered 50 mM KCl, a small amount of protein precipitate is formed that can be removed from the solution by centrifugation at 12000g. In addition, when dimethylsuberimidate cross-linking experiments are performed at low salt concentrations, aggregates larger than hexamers inevitably are generated (Geiselmann et al., 1992).

A radically different behavior is observed if short RNA (or DNA) oligomers (8–20 nucleotide residues in length) are added to rho under conditions of moderate salt concentration (e.g., 50 mM KH_2PO_4). In this case a homogeneous dodecamer of rho is formed. We do not know whether this association state of rho has physiological significance. The stable existence of the rho dodecamer, and the rho to oligonucleotide stoichiometry that is involved, places constraints on the symmetry and assembly pathway of the rho hexamer. These aspects are discussed in the following paper in this issue (Geiselmann et al., 1992). Some of the physical properties of the rho dodecamer are described further below.

A Stable Homogeneous Rho Hexamer

Sedimentation Velocity. In Figure 1 a limiting value of 10.4 S is observed for rho under certain solution conditions. The 10.4 S material predominates in 100–200 mM KCl or in 50 mM KH_2PO_4 at rho concentrations of 0.25–1 mg/mL (5–20 mM in rho protomers). In Figure 2 we show the Van Holde–Weischet analysis of sedimentation data for a solution of 0.3 mg/mL rho in 50 mM KH_2PO_4. The lines in this plot converge at $S_{20,w}$ = 10.4 S, suggesting that the solution may be monodisperse. However, as noted under Materials and Methods, this method of analyzing sedimentation data cannot distinguish between a solution containing a homogeneous species and a heterogeneous system in which two or more associated forms equilibrate rapidly on the time scale of the sedimentation experiment.

Quasielastic Light Scattering. The above problem can be overcome by testing for solute homogeneity with QLS. This technique can detect rapid equilibration between different states of association (Bloomfield & Lim, 1978). QLS experiments were performed on all samples of rho that showed a homogeneous 10.4 S sedimentation boundary. A rapid equilibration between species of different sizes would be revealed by a large "polydispersity index". In each case the observed autocorrelation decay could be fit well by a single-exponential function, suggesting that the sample was homogeneous (see eq 3A). A $D_{20,w}$ value of 3.4×10^{-7} cm^2/s was measured for the 10.4 S species.

Because the autocorrelation function does display single-exponential decay behavior, we are justified in applying the Svedberg equation (eq 4C) to sedimentation and diffusion data collected on the 10.4 S species. The molecular weight estimated from these $S_{20,w}$ and $D_{20,w}$ values using the Svedberg equation is 287 000. This molecular weight is very close to the value of 282 000 that can be calculated for the rho hexamer from the DNA sequence of the gene (see Table I).

Sedimentation Equilibrium. An independent test of molecular weight homogeneity can be provided by sedimentation equilibrium. We conducted sedimentation equilibrium experiments on rho dissolved in 50 mM KH_2PO_4 (pH 7.6). In this buffer rho protein sediments at 10.4 S (see Figure 1). The sedimentation equilibrium data show a linear dependence of ln Δj on r^2 over the entire measurable range of rho concentration. This provides strong evidence that the 10.4 S species is homogeneous. The slope of the ln Δj versus r^2 plot is related to the molecular weight of the associated species by eq 1. From the sedimentation equilibrium data, we estimate the molecular weight of the 10.4 S species to be 286 000, in virtually perfect agreement with the calculated molecular weight of the rho hexamer.

Small-Angle X-ray Scattering. We have also performed SAXS experiments on the 10.4 S material and have constructed Guinier plots to test for solute homogeneity. The 10.4 S material was examined at concentrations of 2.6, 3.9, 5.6, and 7.9 mg/mL in the 50 mM KH_2PO_4 (pH 7.7) buffer. Guinier plots were usually constructed over the 0.08–0.4 nm^{-1} range of the scattering vector. The Guinier plots were linear over the outer 70–90% of this range of the scattering vector but showed some positive curvature at smaller values of q. This positive curvature indicates some degree of association beyond the 10.4 S species at the relatively high rho concentrations used in X-ray scattering experiments. This aggregation is expected on the basis of the sedimentation data of Figure 1. From the linear (outer) portion of the Guinier plots, we estimate that the radius of gyration, R_G, of the 10.4 S species is 50 ± 3 Å.

The intensity of forward scattering from the 10.4 S species was obtained by extrapolation from the linear (outer) portion of the Guinier plot. The forward scattering intensity was compared to that of a 300 000 molecular weight standard (ATCase at a concentration of 4.9 mg/mL). Comparison allows us to estimate the molecular weight of the 10.4 S species. Estimates from two independent experiments gave M = 285 000 at a rho concentration of 3.9 mg/mL, and M = 281 000 at 7.9 mg/mL of rho. These estimates are in excellent agreement with molecular weights for the rho hexamer measured by other techniques and calculated from the gene sequence (see above and Table I).

Small-Angle Neutron Scattering. We also carried out SANS experiments on the 10.4 S material. For rho at a concentration of 5.7 mg/mL in ^2H_2O, the scattering intensity and the contrast were great enough to produce a high quality Guinier plot using neutrons of wavelength 1.3 nm. Thirty measurements of scattering intensity were collected at values of the scattering vector between 0.045 and 0.48 nm^{-1}. In a Guinier plot, the outer 25 points were found to lie on a straight line. The inner five points displayed upward curvature as seen with the X-ray scattering data, again indicating that a small

fraction of the 10.4 S material aggregates at this high concentration of rho (5.7 mg/mL). From the linear (outer) portion of the Guinier plot, we estimate the neutron radius of gyration of the 10.4 S species to be 47 ± 3 Å. We note that the neutron-scattering experiments were performed after extensive dialysis into ^2H_2O. Thus most of the solvent accessible N-bonded and O-bonded protons will have exchanged with the solvent (Ibel & Stuhrmann, 1975). This exchange may account, in part, for the discrepancy between the radius of gyration of the rho hexamer measured by SAXS (50 ± 3 Å) and that measured by SANS (47 ± 3 Å).

The intensity of forward scattering from the 10.4 S species was obtained by extrapolation from the linear (outer) portion of the Guinier plot. The forward scattering intensity was calibrated against the absolute scattering intensity of water measured on the same instrument. This allowed an absolute determination of the molecular weight of the 10.4 S sample using eq 5D. The molecular weight obtained in this way is M = 285 000 ± 25 000 in ^2H_2O.

Shape of the Rho Hexamer

Early electron micrographs (Oda & Takanami, 1972) suggested that the rho hexamer consists of six protomers located at the corners of a regular hexagon, with a "hole" in the center of the structure. More recent electron micrographs, obtained with the techniques of staining–shadowing (Bear et al., 1988) or rapid freezing in amorphous ice (Gogol et al., 1991), are in accord with this finding. However, since electron microscopy can be subject to artifacts of preparation, we wanted to determine the shape of the rho hexamer in solution by an independent technique.

Translational Frictional Coefficient. Hydrodynamic theory allows one to calculate theoretical S and D values for an arbitrary arrangement of protomers in a multimeric structure (eq 4D). Thus one can test whether the observed S and D values of the rho hexamer are consistent with the structure suggested by electron microscopy. To apply eq 4D, values must be assumed for the sedimentation and diffusion coefficients of the protomer. An empirical relation between $S_{20,w}$ and molecular weight has been noted by Van Holde (1975) for many globular proteins of average hydration in dilute solution. This relation predicts values of $S_{20,w}$ = 3.4 S and $D_{20,w} = 7.0 \times 10^{-7}$ cm^2/s for the rho protomer, assuming a spherical shape and an average degree of hydration. The predicted value of $S_{20,w}$ is in good agreement with the sedimentation coefficient measured for the rho protomer at very low rho concentrations [see Seifried et al. (1991)]. Using the theoretical $S_{20,w}$ and $D_{20,w}$ coefficients for the protomer, we employ eq 4D to predict a sedimentation coefficient of 9.6 S and a diffusion coefficient of 3.3×10^{-7} cm^2/s for a regular hexagonal arrangement of such spherical protomers. These calculated values are only 8% and 3% lower than the measured values (see Table I). Thus the measured sedimentation and diffusion coefficients are consistent with the structural model proposed from electron microscopy data. We note, however, that slightly different structures can have virtually identical translational frictional properties (Bloomfield et al., 1967; Van Holde, 1975). Thus we do not attempt to make further inferences about the structure of the rho hexamer from sedimentation and diffusion measurements; we turn instead to other experimental techniques.

Radius of Gyration. A more discriminating test for structure is provided by radius of gyration measurements. R_G can be easily calculated for simple ensembles of spherical subunits, using the parallel axis theorem (eq 6A). For this theoretical calculation, we have assumed a regular hexagonal arrangement of six spheres. Each sphere has a radius of 24 Å, and the centers of the spheres are equally spaced along the perimeter of a circle of radius 45 Å (see Figure 6). Each sphere corresponds to a rho protomer of molecular weight 46 974 and partial specific volume $\bar{v}_2$ = 0.75 cm^3/g. The slight overlap between adjacent spheres reflects our conclusion that the rho hexamer has D_3 symmetry and thus displays some apparent superposition of adjacent protomers when viewed from above and in Figure 6 [see Geiselmann et al. (1992)]. We calculate a radius of gyration of 49 Å for this assemblage. This should be compared to measured values for the rho hexamer of 50 ± 3 Å in SAXS and 47 ± 3 Å in SANS. Again, we conclude that the experimental data agree well with a "regular hexagon" model for rho.

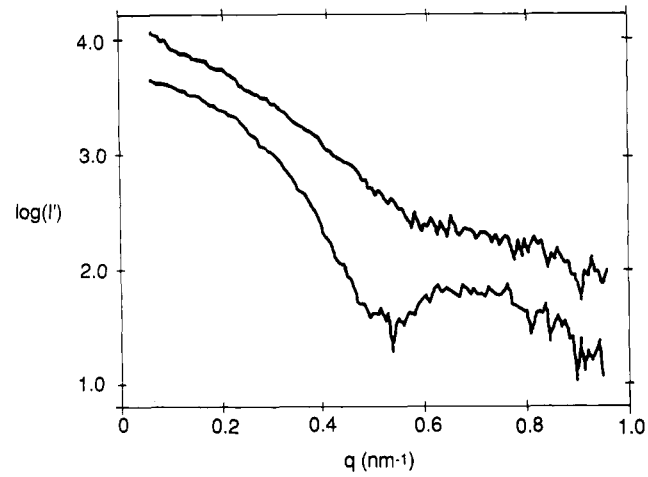

FIGURE 3: X-ray scattering curves for the rho hexamer and rho dodecamer. The logarithm of the corrected scattering intensity is plotted as a function of the scattering vector. (Top) The scattering curve of a 7.8 mg/mL solution of rho hexamer in 50 mM KH_2PO_4 (pH 7.0). (Bottom) The scattering curve of a 7.1 mg/mL solution of rho dodecamer in 50 mM KH_2PO_4 (pH 7.7). A saturating amount of $(dC)_{20}$ is bound to the rho dodecamer. The vertical scale has arbitrary units.

X-Ray and Neutron-Scattering Curves beyond the Guinier Region. More information about the low-resolution solution structure of a macromolecule can be obtained by examining SAXS or SANS curves beyond the Guinier region. The scattering curves should have sufficient detail to determine if the regular hexagon model is appropriate for rho in solution.

Figure 3 (top curve) shows the X-ray scattering curve of the rho hexamer at a rho concentration of 7.9 mg/mL in 50 mM KH_2PO_4. The logarithm of the corrected scattering intensity is plotted as a function of the scattering vector. A secondary scattering shoulder is found at approximately q = 0.8 nm^{-1}. A cusp is located between the primary peak and the shoulder, at approximately q = 0.6 nm^{-1}. Scattering curves with essentially the same features (but with greater noise) were also observed for samples of the rho hexamer at concentrations of 5.9, 3.9, and 2.6 mg/mL (data not shown). The equivalence of these scattering curves indicates that the "interparticle interference" effect (Pilz, 1981) is not very significant over the 2.6–7.9 mg/mL concentration range.

In Figure 4 (top curve) we present the corresponding neutron-scattering curve of the rho hexamer at a protein concentration of 5.6 mg/mL in 50 mM KH_2PO_4 in ^2H_2O. Again the logarithm of the corrected scattered intensity is plotted against q. As in the X-ray profile (Figure 3, top), we see a secondary scattering peak as a "shoulder" on the primary peak. A shallow minimum between the primary and secondary peaks is observed at q = 0.75 nm^{-1}. The neutron-scattering profile in ^2H_2O is qualitatively similar to the X-ray profile shown in

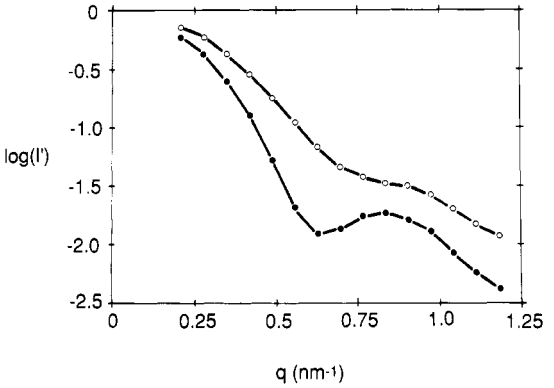

FIGURE 4: Neutron-scattering curves for the rho hexamer and dodecamer. (Top) The scattering curve of a 5.7 mg/mL solution of the rho hexamer in 50 mM KH_2PO_4 (pD 7.9) in ^2H_2O. (Bottom) The scattering curve of a 5.3 mg/mL solution of the rho dodecamer in the same buffer. A saturating amount of $(dC)_{20}$ is bound to the rho dodecamer. The vertical scale has arbitrary units.

Figure 3 (top), lending additional support to the "regular hexagon" model. In comparison to the X-ray profile, the SANS profile is flatter and shifted somewhat toward higher values of the scattering vector. This shift may result from the fact that X-ray scattering and neutron scattering are affected differently by the internal inhomogeneities (structure) of a macromolecule, especially when the solvent is ^2H_2O.

Theoretical scattering curves for three different hexameric arrangements of spherical protomers are presented in Figure 5 (top). Each protomer is represented as a homogeneous sphere of radius 32 Å. (A sphere equivalent to a rho protomer in mass and partial specific volume has radius 24 Å. A larger radius was chosen for the calculation of approximate scattering curves in order to simulate a rho protomer that is not exactly spherical in shape. The shapes of the scattering curves remain similar when changing the radii within this range.) The hexameric arrangements that we have considered are as follows: (i) the "regular hexagon with central hole" that is suggested by the electron micrographs of rho; (ii) the "hexamer octahedron", consisting of two trimers of equivalent geometry superimposed in a staggered array (Klotz et al., 1975); and (iii) a linear arrangement of six protomers. The distance between the centers of the adjacent protomers is 45 Å in each case. The calculated curves are only approximations because a slight overlap between spheres was used. However, the approximations are good enough for qualitative conclusions to be drawn. The experimental data agree best with the theoretical curve corresponding to model (i). This further supports the regular hexagonal model for the rho hexamer in solution.

A Dodecamer of Rho Is Generated by Binding of Short Oligonucleotide Ligands

When a rho solution is titrated with short oligomers of RNA or DNA such as $(rC)_{10-20}$ or $(dC)_{10-20}$, a discrete species is formed that displays $S_{20,w} \simeq 17.5$ S. In sedimentation equilibrium, sedimentation velocity, and quasielectric light scattering, this species appears most homogeneous at a stoichiometry of one oligonucleotide for every two rho monomers. QLS yields a diffusion coefficient of 2.8×10^{-7} cm^2/s for this species.

The 17.5 S species appears homogeneous by the following criteria: (i) in QLS experiments we observe a low polydispersity index and no dependence of the observed $D_{20,w}$ values on scattering angle; (ii) analysis of the velocity sedimentation boundary by the Van Holde–Weischet (1978) technique yields S_{app} vs $t^{-1/2}$ lines that converge as $t^{-1/2}$ approaches zero; (iii)

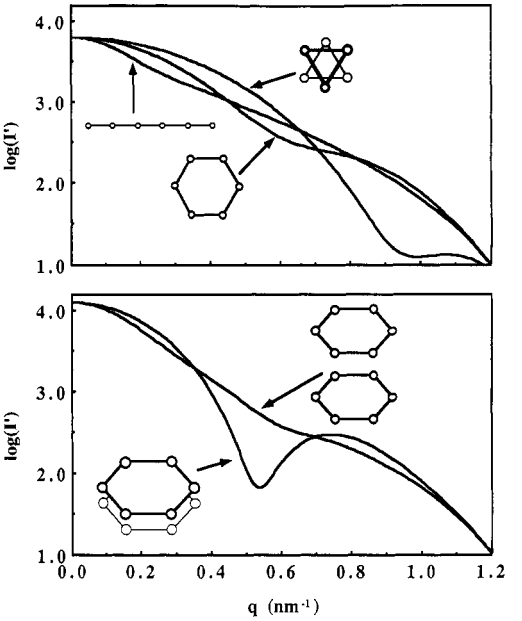

FIGURE 5: Theoretical scattering curves for the rho hexamer and dodecamer. (Top) Three possible models of the rho hexamer are considered. Calculations are according to eqs 7B and 7C. The vertical scale has arbitrary units. (Bottom) Two possible models of the rho dodecamer are considered. Each model is built from two regular planar hexamers. Calculations are according to eqs 7B and 7C. The vertical scale has arbitrary units.

in sedimentation equilibrium experiments we observe a linear dependence of ln Δj on r^2; and finally (iv) linear Guinier plots are obtained in SAXS and SANS experiments.

Since the 17.5 S species appears homogeneous, the Svedberg equation can be applied to our sedimentation velocity and diffusion data to yield a molecular weight of 540 000. In this calculation, we use data obtained by titration with $(dC)_{20}$ ligands. We assume that $\bar{v}_2 = 0.74$ cm^3/g, computed as a weight average value of rho (0.75 cm^3/g) and $(dC)_{20}$ (0.53 cm^3/g). The molecular weight of the 17.5 S species measured by the sedimentation equilibrium technique is 540 000 (again assuming that $\bar{v}_2 = 0.74$ cm^3/g). Values of $M = 576\,000 \pm 50\,000$ and $M = 600\,000 \pm 50\,000$ are obtained from the extrapolated forward scattering intensity of X-rays and of neutrons in ^2H_2O, respectively. On the basis of the DNA sequence of the rho gene and the known molecular weights of the oligonucleotide ligands, we expect a molecular weight of 583 000 for a rho dodecamer complexed with six $(dC)_{20}$ ligands. Our experimental results for the rho dodecamer are thus also in excellent agreement with theoretical values.

A homogeneous dodecamer of rho containing six molecules of $(dC)_{20}$ was examined by SAXS and SANS to learn more about its quaternary structure. Figures 3 (bottom) and 4 (top) are plots of scattering curves for X-rays and for neutrons in ^2H_2O, respectively. The logarithm of the corrected scattering intensity is plotted as a function of the scattering vector. The scattering curves are similar to those obtained for the rho hexamer in Figures 3 (top) and 4 (top), except that the minimum between the first and second peak, and the intensity of the second peak, are much more pronounced for the dodecamer.

Theoretical scattering curves for two different arrangements of hexamer pairs (i.e., dodecamers) are shown in Figure 5 (bottom). The observed scattering curves appear most consistent with a structure in which two planar hexamers are stacked so that the two central "holes" are aligned. Such a structure has also been seen directly by cryoelectron microscopy (Gogol et al., 1991).

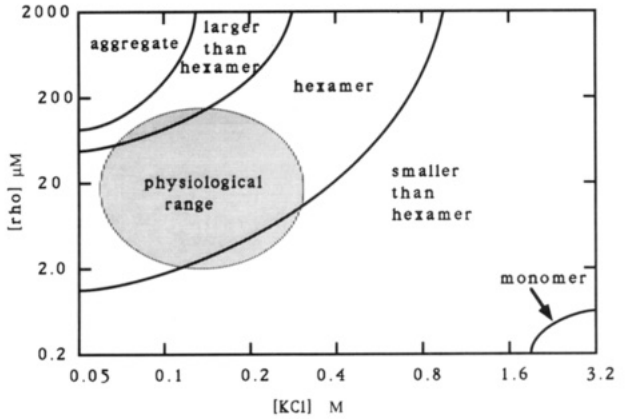

FIGURE 6: Semiquantitative "phase diagram" of the association states of rho. Our best approximation to "physiological" conditions is indicated by the shaded area. The conditions under which rho is predominantly a hexamer are indicated by the zone labeled "hexamer". We assume that the monomeric association state exists at low concentrations of rho, even though we did not observe this state directly in the experiments reported in this paper [however, see Seifried et al. (1991)].

Information about the average position of the $(dC)_{20}$ ligands within the rho dodecamer can be gained by examining how the radius of gyration of the dodecamer obtained by neutron scattering is affected by varying the solvent scattering length density. Preliminary results suggest that the DNA ligands are located toward the outside of the dodecamer, rather than in the central hole (data not shown).

Discussion

In this paper we have shown that *E. coli* transcription termination factor rho can exist in a variety of association states. Two major variables that affect the equilibrium distribution between these states are the concentration of rho and the nature of the ionic environment. Changes in pH between 7 and 10 have only minor effects on the state of association of rho, though we find that the protein precipitates when the pH is lowered below 6 (data not shown). The effects of protein concentration and KCl or KH_2PO_4 concentration on rho association states are summarized in Figure 6 in the form of a semiquantitative "phase diagram". We have characterized the single most prevalent species in this phase diagram by a variety of physical techniques and have shown it to be a nearly homogeneous hexamer (Table I). By applying a combination of electron microscopic, hydrodynamic, and X-ray and neutron-scattering techniques, we have concluded that the protomers of this hexamer are located at the corners of a regular hexagon.

X-ray scattering curves of the rho hexamer are in reasonable agreement with theoretical scattering curves when the regular hexagonal geometry of Figure 7 is assumed. In calculating the theoretical scattering curves, each protomer is assumed to be spherical with $M = 46\,100$ and $\bar{\nu}_2 = 0.75$ cm^3/g. This leads to a calculated radius of 24 Å for each protomer sphere. The theoretical curves can be made to fit the SAXS data better by using spheres of a larger radius than 24 Å in the calculations. This might indicate that, in reality, the rho protomers are somewhat ellipsoidal rather than being perfectly spherical in shape.

Neutron-scattering curves of the rho hexamer are reasonably consistent with both the X-ray scattering curves and the theoretical models. However two discrepancies should be noted, namely, that the R_G is found to be 47 ± 3 Å instead of 50 ± 3 Å and that the neutron-scattering curves appear "flattened" and shifted toward higher q values relative to the

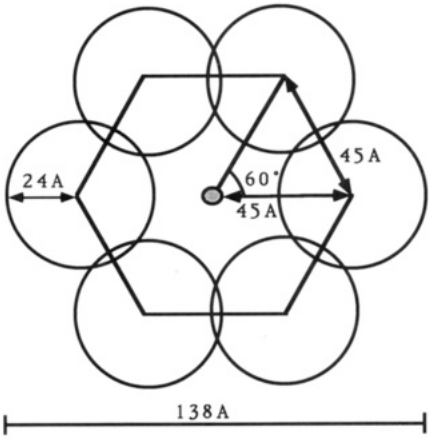

FIGURE 7: Geometric model for the rho hexamer. Protomers of rho are represented by spheres of radius 24 Å (corresponding to protomers with $M = 46\,100$ and $\bar{\nu}_2 = 0.75$ cm^3/g). This proposed geometry of the rho hexamer is consistent with data from X-ray scattering, neutron scattering, and electron microscopy. The calculated radius of gyration of this structure is 49 Å.

X-ray scattering curves. An exchange of protons might lead to a smaller apparent value of R_G and a slightly different scattering curve than is observed with X-rays. The neutron-scattering curves that we have obtained are better modeled by assuming smaller protomers and shorter distances between their centers of mass. Further experiments of greater precision will be needed to settle these points.

A homogeneous dodecamer of rho is formed by end point titration of a rho solution with a short oligomer of RNA or DNA. The dodecamer has a stoichiometry of two rho protomers for each oligonucleotide ligand. This dodecamer appears to be formed by the coplanar stacking of two rho hexamers [see also Gogol et al. (1991)]. The possible significance of this dodecamer will be discussed elsewhere (Geiselmann et al., manuscript in preparation).

To better understand the physiological significance of the association states depicted in Figure 6, we must ask what concentrations of rho and salt are likely to be present in vivo. Rho is thought to represent approximately 0.1–0.15% of the total soluble protein within the cell (Imai & Shigesada, 1978). If we assume that the total weight of protein per cell is 2.8×10^{-13} g (Ingraham et al., 1983), then there should be approximately 4000–6000 rho protomers per cell, or approximately one rho hexamer for every two or three molecules of RNA polymerase [see Imai and Shigesada (1978)]. If we assume the volume of a typical *E. coli* cell to be 10^{-15} L, then the in vivo concentration of rho monomers should be about 6 μM. We note that this calculation neglects the effects of "macromolecular crowding" (Minton, 1981) and thus should be regarded as a lower limit estimate of the effective concentration of rho in vivo. Our sedimentation experiments span the 5–50 μM rho protomer concentration range. Thus our measurements were made at marginally higher concentrations of rho than are estimated to be present in the cell. To compensate, however, the *effective* concentration of rho within the cell is expected to be somewhat greater than the above estimate because of macromolecular crowding effects.

In *E. coli* the potassium ion concentration varies between 0.1 and 1 M (Richey et al., 1987), and the main physiological anions are likely to be the phosphate groups of the DNA and RNA. We observe that a reasonably homogeneous rho hexamer exists between 0.1 and 0.5 M KCl (Figure 1). We have carefully measured the partial specific volume of the rho protein in 0.1–0.5 M KCl and in 50 mM KH_2PO_4 (Table I). Our experimental values of $\bar{\nu}_2$ are in good agreement with

calculations from amino acid composition. This agreement suggests that rho does not bind unusually large amounts of water or salt. Thus variations in salt concentration within the cell are unlikely to produce large changes in the state of association of the rho protein.

Taken together, these data and arguments suggest that physiological conditions within the *E. coli* cell may fall within the gray oval shown in Figure 6. Thus we conclude that rho protein is likely to exist predominantly as a hexamer in vivo. We emphasize, however, that the hexamer most likely will participate in labile equilibria involving both higher and lower association states [Figure 1 and Seifried et al. (1991)]. Rho molecules bind to a polynucleotide as hexamers (Bear et al., 1988; Geiselmann et al., manuscript in preparation). In the following paper in this issue (Geiselmann et al., 1992), we augment these data by characterizing the interactions between rho protomers in the hexamer in order to define the symmetry of this species. The quaternary structure of the rho hexamer must be completely defined before a plausible molecular model can be proposed for the function of rho protein as a DNA–RNA helicase in transcript termination (Geiselmann et al., manuscript in preparation).

ACKNOWLEDGMENTS

We thank the Biotechnology Laboratory of the University of Oregon for synthesis of $(dC)_{10}$ and $(dC)_{20}$, the Shared Laser Facility of the University of Oregon for use of QLS equipment, and Dr. K. E. Van Holde (Oregon State University) for the use of his model E analytical ultracentrifuge. We also thank Drs. Patrice Vachette and Annette Tardieu for help with the experiments at LURE and for preliminary model calculations of the high-angle X-ray scattering curves in terms of hexamers and dodecamers. In addition, we are grateful to Drs. John Schellman (University of Oregon) and Henryk Eisenberg (Weizmann Institute) for advice on densimetry measurements, to Dr. Guiseppe Zaccai of the Institut Laue-Langevin in Grenoble, France, for discussion of scattering experiments, to Dr. Walter Baase of the University of Oregon for discussion of QLS experiments, and to Dr. Stanley J. Gill (deceased) of the University of Colorado for discussion of self-associating macromolecular systems.

REFERENCES

Adler, A., Grossman, L., & Fasman, G. D. (1967) *Proc. Natl. Acad. Sci. U.S.A. 57*, 423–430.

Bear, D. G., & Peabody, D. S. (1988) *Trends Biochem. Sci. 13*, 343–347.

Bear, D. G., Hicks, P. S., Escudero, K. W., Andrews, C. L., McSwiggen, J. A., & von Hippel, P. H. (1988) *J. Mol. Biol. 199*, 623–636.

Berne, B. J., & Pecora, R. (1976) *Dynamic Light Scattering*, John Wiley and Sons, New York.

Bloomfield, V. A., & Lim, T. K. (1978) *Methods Enzymol. 48*, 415–494.

Bloomfield, V. A., Dalton, W. O., & Van Holde, K. E. (1967) *Biopolymers 5*, 135–148.

Boulin, C., Kempf, R., Koch, M. H. J., & McLaughlin, S. M. (1986) *Nucl. Instrum. Methods Phys. Res., Sect. A 249*, 399–407.

Calmettes, P., Eisenberg, H., & Zaccai, G. (1987) *Biophys. Chem. 26*, 279–290.

Calmettes, P., Girault, G., Berger, G., & Galmiche, J. M. (1989) *Physica B 156 and 157*, 481–484.

Chen, C. A., Galluppi, G. R., & Richardson, J. P. (1986) *Cell 46*, 1023–1028.

Chervenka, C. H. (1965) *A Manual of Methods for the Analytical Ultracentrifuge*, Spinco Division, Beckman Instruments, Palo Alto, CA.

Chu, B. (1974) *Laser Light Scattering*, Academic Press, New York.

Cotton, J. P. (1984) *Internal Report no.* 758, Laboratoire Léon Brilloun, CEN Saclay, Gif-sur-Yvette, France.

Depautex, C., Desvignes, C., Feder, P., Lemonnier, M., Bosshard, R., Leboucher, P., Dagneaux, D., Benoit, J. P., & Vachette, P. (1987) *LURE Rapport d'activité pour la periode Aout 1985–Avril 1987*, p 87, doc. CEN Saclay.

Dombrowski, A. J., & Platt, T. (1988) *Proc. Natl. Acad. Sci. U.S.A. 85*, 2538–2542.

Edelhoch, H. (1967) *Biochemistry 6*, 1948–1954.

Finger, L. R., & Richardson, J. P. (1981) *Biochemistry 20*, 1640–1645.

Finger, L. R., & Richardson, J. P. (1982) *J. Mol. Biol. 156*, 203–219.

Gabriel, A., Dauvergne, F., & Rosenbaum, G. (1978) *Nucl. Instrum. Methods 152*, 191–194.

Geiselmann, J., Seifried, S. E., Yager, T. D., Liang, C., & von Hippel, P. H. (1992) *Biochemistry* (following paper in this issue).

Gill, S. C., & von Hippel, P. H. (1989) *Anal. Biochem. 182*, 319–326.

Gogol, E. P., Seifried, S. E., & von Hippel, P. H. (1991) *J. Mol. Biol. 221*, 1127–1138.

Guinier, A. C., & Fournet, G. (1955) *Small Angle Scattering of X-rays*, Wiley, New York.

Imai, M., & Shigesada, K. (1978) *J. Mol. Biol. 120*, 451–466.

Ingraham, J. L., Maaloe, O., & Neidhardt, F. C. (1983) *Growth of the Bacterial Cell*, Sinauer, Sunderland, MA.

Klotz, I. M., Darnall, D. W., & Langerman, N. R. (1975) in *The Proteins* (Neurath, H., & Hill, R. L., Eds.) 3rd. ed., Vol. 1., pp 293–414, Academic Press, New York.

Koppel, D. E. (1972) *J. Chem. Phys. 57*, 4814–4820.

Kunz, W., Calmettes, P., & Turq, P. (1990) *J. Chem. Phys. 92*, 2367–2373.

Lane, A. N. (1982) *J. Theor. Biol. 97*, 511–527.

Lee, J. C., & Timasheff, S. N. (1974) *Biochemistry 13*, 257–265.

Minton, A. P. (1981) *Biopolymers 20*, 2093–2120.

Morgan, W. D., Bear, D. G., & von Hippel, P. H. (1983a) *J. Biol. Chem. 258*, 9553–9564.

Morgan, W. D., Bear, D. G., & von Hippel, P. H. (1983b) *J. Biol. Chem. 258*, 9565–9574.

Morgan, W. D., Bear, D. G., & von Hippel, P. H. (1984) *J. Biol. Chem. 259*, 8664–8671.

Morgan, W. D., Bear, D. G., Litchman, B., & von Hippel, P. H. (1985) *Nucleic Acids Res. 13*, 3739–3754.

Mott, J. E., Grant, R. A., Ho, Y., & Platt, T. (1985) *Proc. Natl. Acad. Sci. U.S.A. 82*, 88–92.

Noelken, M. E., & Timasheff, S. N. (1967) *J. Biol. Chem. 242*, 5080–5085.

Oda, T., & Takanami, M. (1972) *J. Mol. Biol. 71*, 799–802.

Platt, T. (1986) *Annu. Rev. Biochem. 55*, 337–372.

Platt, T., & Bear, D. G. (1983) in *Gene Function in Prokaryotes* (Beckwith, J., Davies, J., & Gallant, J. A., Eds.) pp 123–161, Cold Spring Harbor Laboratory Press, Cold Spring Harbor, NY.

Pilz, I. (1982) in *Small Angle X-ray Scattering* (Glatter, O., & Kratky, O., Eds.) pp 239–293, Academic Press, New York.

Pinkham, J. L., & Platt, T. (1983) *Nucleic Acids Res. 11*, 3531–3545.

Reisbig, R. R., & Hearst, J. E. (1981) *Biochemistry 20*, 1907-1918.
Reisler, E., & Eisenberg, H. (1969) *Biochemistry 8*, 4572-4576.
Richey, B., Cayley, D. S., Mossing, M. C., Kolka, C., Anderson, C. F., Farrar, T. C., & Record, M. T., Jr. (1987) *J. Biol. Chem. 262*, 7157-7164.
Schachman, H. K. (1959) *Ultracentrifugation in Biochemistry*, Academic Press, New York.
Seifried, S. E., Wang, Y., & von Hippel, P. H. (1988) *J. Biol. Chem. 263*, 13511-13514.
Seifried, S. E., Bjornson, K. P., & von Hippel, P. H. (1991) *J. Mol. Biol. 211*, 1139-1151.
Sharp, J. A., & Platt, T. (1984) *J. Biol. Chem. 259*, 2268-2273.
Stockel, P., May, R., Strett, I., Zdenka, C., Hoppe, W., Heumann, H., Zillig, W., Crespi, H. L., Katz, J. J., & Ibel, K. (1979) *J. Appl. Crystallogr. 12*, 176.
Van Holde, K. E. (1967) *Fractions*, Vol. 1, pp 1-10, Spinco Division, Beckman Instruments, Palo Alto, CA.
Van Holde, K. E. (1975) in *The Proteins* (Neurath, H., & Hill, R. L., Eds.) 3rd, ed., Vol. 1, pp 225-291, Academic Press, New York.
Van Holde, K. E., & Weischet, W. O. (1978) *Biopolymers 17*, 1387-1403.
von Hippel, P. H., Bear, D. G., Morgan, W. D., & McSwiggen, J. A. (1984) *Annu. Rev. Biochem. 53*, 389-446.
Weast, R. C. (1978) *Handbook of Chemistry and Physics*, CRC Press, Cleveland, OH.
Yager, T. D., & von Hippel, P. H. (1987) in *E. coli and S. typhimurium: Cellular and Molecular Biology* (Neidhardt, F. C., Ingraham, J. L., Low, K. B., Magasanik, B., Schaechter, M., & Umbarger, H. E., Eds.) pp 1241-1275, American Society for Microbiology, Washington, DC.

Physical Properties of the *Escherichia coli* Transcription Termination Factor Rho. 2. Quaternary Structure of the Rho Hexamer†

Johannes Geiselmann,‡ Steven E. Seifried, Thomas D. Yager,§ Cheryl Liang,‖ and Peter H. von Hippel*
Institute of Molecular Biology and Department of Chemistry, University of Oregon, Eugene, Oregon 97403
Received May 13, 1991; Revised Manuscript Received August 22, 1991

ABSTRACT: Under approximately physiological conditions, the transcription termination factor rho from *Escherichia coli* is a hexamer of planar hexagonal geometry [Geiselmann, J., Yager, T. D., Gill, S. C., Calmettes, P., & von Hippel, P. H. (1992) *Biochemistry* (preceding paper in this issue)]. Here we describe studies that further define the quaternary structure of this hexamer. We use a combination of chemical cross-linking and treatment with mild denaturants to show that the fundamental unit within the rho hexamer is a dimer stabilized by an isologous (or pseudoisologous) bonding interface. Three identical dimers of rho interact via a second type of isologous bonding interface to yield a hexamer with C_3 or D_3 symmetry. Cross-linking and denaturation experiments definitely rule out C_6 and C_2 symmetry for the rho hexamer. Data from fluorescence quenching, lifetime, and energy transfer experiments also argue against C_2 symmetry. The *simplest* symmetry assignment that is not contradicted by any experimental data is D_3; thus we conclude that the rho hexamer has D_3 symmetry. We also consider the positioning of the binding sites for RNA and ATP relative to the coordinate reference frame of the D_3 hexamer. Fluorescence energy transfer data are presented and integrated with data from the literature to arrive at a self-consistent model for the quaternary structure of the rho hexamer.

The quaternary structure of a protein must be known before its function can be established in molecular terms. Four types of information define the quaternary structure of an oligomeric protein. These are (i) the self-association state, (ii) the geometric arrangement of protomers in the associated state, (iii) the symmetry assignment, and (iv) the disposition on the protomer of unique cofactor- or substrate-binding sites relative to the coordinate reference frame of the protein oligomer.

In the preceding paper in this issue (Geiselmann et al., 1992), we studied the association states of the *Escherichia coli* transcription termination factor rho as a function of protein concentration, ionic environment, and binding of oligonucleotide cofactors. By a combination of physicochemical techniques, we showed that in solution the rho protomer is involved in various self-association equilibria [see also Seifried et al. (1991)]. The states of this self-associating system were summarized in the form of a phase diagram with axes defined in terms of protein and salt concentration. Depending on experimental conditions, the average association state of rho was found to range from monomers up to indefinite aggregates.

We also showed (Geiselmann et al., 1992) that under approximately physiological conditions (10-40 μM rho protomers and 50-200 mM KCl) the rho protein exists in a homogeneous

† Portions of this work have been submitted (by J.G.) to the Graduate School of the University of Oregon in partial fulfillment of the requirements for the Ph.D. degree in Chemistry. These studies were supported in part by USPHS Research Grants GM-15792 and GM-29158 (to P.H.v.H.), by NIH Individual Postdoctoral Fellowship GM-10227 (to TDY), and by a grant from the Lucille P. Markey Charitable Trust. P.H.v.H. is an American Cancer Society Research Professor of Chemistry.
* To whom correspondence should be addressed.
‡ Present address: Unité de Physicochimie des Macromolécules Biologiques, Institut Pasteur, 25 rue du Dr. Roux, 75724 Paris Cedex 15, France.
§ Present address: NSF Center for Molecular Biotechnology, Division of Biology (139-74), California Institute of Technology, Pasadena, CA 91125.
‖ Present address: Department of Chemistry, University of California at Riverside, Riverside, CA.

0006-2960/92/0431-121$03.00/0